J Therm Anal Calorim (2010) 100:43–49
DOI 10.1007/s10973-009-0160-y

Kinetics of formation of barium tungstate in equimolar powder mixture of $BaCO_3$ and WO_3

Thermogravimetric and spectroscopic studies

Latifa A. Al-Hajji · Muhammad A. Hasan · Mohamed I. Zaki

Received: 6 March 2009 / Accepted: 16 April 2009 / Published online: 1 September 2009

Abstract The formation of Barium monotungstate ($BaWO_4$) particles in equimolar powder mixtures of $BaCO_3$ and WO_3 was examined under isothermal and non-isothermal conditions upon heating in air at 25–1200 °C, using thermogravimetry. Concurrence of the observed mass loss (due to the release of CO_2) to the occurrence of the formation reaction was evidenced. Accordingly, the extent of reaction (x) was determined as a function of time (t) or temperature (T). The x–t and x–T data thus obtained were processed using well established mathematical apparatus and methods, in order to characterize nature of reaction rate-determining step, and derive isothermal and non-isothermal kinetic parameters. Moreover, the reaction mixture quenched at various temperatures (600–1,000 °C) in the reaction course was analyzed by various spectroscopic and microscopic techniques, for material characterization. The results obtained indicated that the reaction rate may be controlled by unidirectional diffusion of WO_3 species across the product layer ($BaWO_4$), which was implied to form on the barium carbonate particles. The isothermally determined activation energy (118–125 kJ/mol) was found to be more credible than that (245 kJ/mol) determined non-isothermally.

Keywords Barium tungstate · Formation in the solid state · Kinetic analysis · Physicochemical characterization · Reaction model

L. A. Al-Hajji · M. A. Hasan
Chemistry Department, Faculty of Science, Kuwait University, P.O. Box 5969, 13060 Safat, Kuwait

M. I. Zaki (✉)
Chemistry Department, Faculty of Science, Minia University, El-Minia 61519, Egypt
e-mail: mizaki@link.net

Introduction

Stoichiometric barium monotungstate (i.e. $BaWO_4$) is distinct amongst analogous barium metalates (e.g., molybdate, titanate and chromate) by its emission of blue or green luminescence [1, 2] and, hence, importance to the electro-optical industry. The wavelength and intensity of the luminescence exhibited have been found to depend largely on the preparation conditions applied [2]. Therefore, various preparation methods have been probed including wet [3–6] and dry [7–11] techniques. Though the "dry methods have been found inferior to the "wet" ones for being more energy and time demanding, yet this can well be sobered via kinetic and mechanistic assessments of the solid-state reactions involved [12].

Accordingly, the present investigation was focused on the preparation of $BaWO_4$ via solid-state reaction(s) in an equimolar, loose powder mixture of $BaCO_3$ and WO_3, an approach [13–16]) that has been infrequently used to obtain the targeted material. The reaction was followed thermogravimetrically, and the fraction of reaction completed (x) as a function of temperature (T) or time (t), was processed using algorithms of well established kinetic models [13–19] in order to derive non-isothermal and isothermal reaction kinetic parameters. Then, the kinetic parameters were discussed on basis of physico-chemical modifications conceded by the reaction mixture, so as to assess the reaction mechanism.

Experimental

Reactants

$BaCO_3$ and WO_3, 99.5% pure products of Aldrich (USA), were ground to $\leq$120 mesh, mixed in equimolar quantities

by first tumbling the two powders and, then, blending with mortar and pestle for 30 min, in order to warrant homogeneity. Portions of the separate and mixed reactants were calcined at some selected temperatures (for 3 h in a static atmosphere of air), and the products were quenched to room temperature (RT) prior to storing over silica gel till further use. For clarity, the uncalcined reactants' mixture is denoted below $BaWO_x$(RT), whereas, for instance, $BaWO_x$ (850) means its 850 °C calcination product.

Thermogravimetry

Thermogravimetry (TG) was carried out in a dynamic atmosphere of air (30 cm^3/min), using a model TGA-50H Shimadzu (Japan) automatically recording thermobalance. For isothermal measurements, the mass change was followed (continuously) at the set temperature for 3 h, whereas for non-isothermal measurements, the mass change was recorded on heating up to 1,200 °C at four different rates (Φ): 10, 20, 35 and 50 °C/min. Data acquisition and handling were facilitated by an on-line workstation (TA-50WS, Shimadzu), and evolved gas analysis by an on-line mass analyzer (a model Thermostar Balzars quadrupole mass analyzer, Zwitzerlands).

Kinetic analysis

Assuming that the release of CO_2 is concurrent to the tungstate formation, the consequent TG-determined mass loss, whether isothermally (as a function of time (t)) or non-isothermally (as a function of temperature (T)), was used to calculate the fraction of reaction completed (x), $x = (m_o–m_{t\ or}\ m_T)/(m_o–m_\infty)$, where m_o is the initial mass, m_t or m_T is the mass at a given time or temperature, and m_∞ is the theoretical mass at reaction completion.

The isothermal **x–t** data were processed using a computer-oriented kinetic analysis based on rate law equations (Table 1) corresponding to the indicated four different models for product growth. On the other hand, the non-isothermal **x–T** data were processed using installed standard software (TGA Kinetic Analysis, Shimadzu) to run the mathematical algorithm of Ozawa's method [14–16].

Characterization techniques

X-ray powder diffractometry (XRD) was carried out at room and higher temperatures, using a Siemens D5000 diffractometer (Germany) equipped with Ni-filtered CuK_α radiation ($\lambda = 1.5418$ Å, 40 kV and 30 mA), and a high-temperature attachment (Bühler's HDK S1, Germany). Infrared (IR) spectra were taken of KBr-supported test samples (<1 mass %) in the frequency range 4,000–400 cm^{-1} (at the resolution of 5.2 cm^{-1}), using a Perkin–Elmer System 2,000 FT–IR spectrometer (Germany). Laser-Raman (LRa) spectra were taken of lightly compacted test samples, at 3,600–200 cm^{-1} and the resolution of 0.2 cm^{-1}, using a Perkin–Elmer System 2000 FT-Ra spectrometer equipped with a near infrared diode pumped Nd:YAG laser ($\lambda = 1.064$ μm and 50–100 mW). For morphological and elemental microprobing of test samples, a model JSM-6300 Jeol scanning electron microscope (SEM, Japan) equipped with a LINK's exl II Oxford energy dispersive spectrometer (EDS, U.K.) was employed.

Results and discussion

Concurrence of mass loss to reaction rate

Figure 1 shows $BaCO_3$ to be thermally stable to heating in air up to 943 °C, at which temperature it commences to

Table 1 Kinetic models for solid-state reactions and corresponding isothermal rate law equations [13, 17, 19]

Kinetic model	Rate law equation[a]	Equation
Diffusion		
Jander (J)	$k_J = [1 - (1 - x)^{1/3}]^2$	1
Kroger–Ziegler (KZ)	$k_{KZ} \ln t = [1 - (1 - x)^{1/3}]^2$	2
Zhuravlev–Lesokhin–Templ'man (ZLT)	$k_{Z\ tLT} = [1/(1 - x))^{1/3} - 1]^2$	3
Ginstling–Brounshtein (GB)	$k_{GB}\ t = 1 - 2x/3 - (1 - x)^{2/3}$	4
Dunwald–Wagner (DW)	$k_{DW}\ t = \ln [6/(\pi^2(1 - x))]$	5
Phase boundary		
Sphere (PB-Sph)	$k_{Sph}\ t = 1 - (1 - x)^{1/3}$	6
Cylinder (PB-Cyl)	$k_{Cyl}\ t = 1 - (1 - x)^{1/2}$	7
Cube (PB-Cub)	$x = 8(k_{Cub})^3t^3 - 12(k_{Cub})^2t^2 + 6(k_{Cub})t$	8
Nuclei Growth (NG)	$\ln (1 - x) = -(k_{NG}\ t)^m$	9
Order of Reaction (RO)	$dx/dt = k_{OR}\ (1 - x)^n$	10
	$k_{OR}\ t = (1/(1 - n))[1 - (1 - x)^{1 - n}]$	11

[a] x Fraction of reaction completed (extent of conversion); n Order of reaction; m Exponent

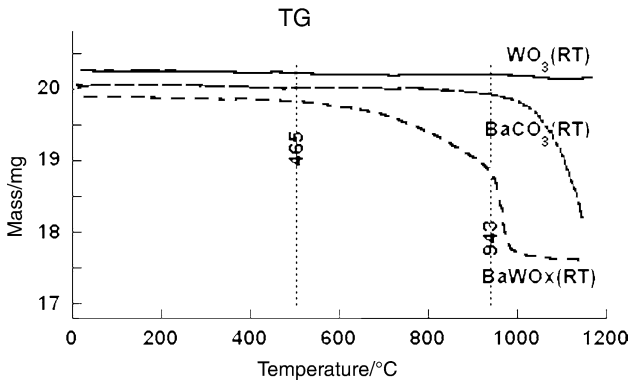

Fig. 1 Non-isothermal TG curves obtained upon heating (at 20 °C/min and 30 cm^3 air/min) of separate and equimolar-mixed powders of $BaCO_3$ and WO_3

suffer mass loss due to thermal decomposition. On the other hand, WO_3 is shown to be mass invariant to heating up to 1,200 °C, whereas $BaWO_x$(RT) is shown to be mass invariant to heating up to 465 °C, followed by a two-step mass loss: (i) a gradual loss (4.3%) occurring at 465–943 °C, and (ii) a very steep loss (5.8%) at 943–990 °C.

It is worth noting, that an on-line gas analysis of volatile decomposition products of $BaCO_3$ and $BaWO_x$(RT) detected nothing, but CO_2 molecules, whereas XRD analysis of the solid products detected BaO (and minority BaO_2) for the former material only. Thus, it is evident that the mass loss conceded by $BaWO_x$(RT) at 465–943 °C is due only to chemical reaction between $BaCO_3$ and WO_3. The fact that the solid product of $BaWO_x$(RT) at 750 °C was found by XRD to be void of separate BaO (or BaO_2) phase, may indicate that the influence of WO_3 is chemical and not catalytic. Accordingly, the mass loss conceded by $BaWO_x$(RT) at 465–943 °C (=10.1%) is concurrent and very close to that (10.25%) expected for the formation of $BaWO_x$ product having a 1:1 BaO:WO_3 composition.

Reaction kinetic analysis and parameters

Based on the TG curve obtained for BaWOx(RT), Fig. 1, the reaction course was TG-examined isothermally at four different temperatures in the range 700–850 °C. Then, four sets of *x–t* data were derived and analyzed using the isothermal rate law equations set out in Table 1. Then rate constant values were calculated and plotted as a function of "*x*". Some of the plots of "*k* versus *x*" for the reaction at 800 °C are shown in Fig. 2. Plots showing "*k*" to depend on the value of "*x*" would rule out the corresponding rate law equations from being appropriate for describing the reaction rate. Accordingly, the relationships exhibited in Fig. 2 help realizing that both Jander (J) and Ginstling–Brounshtein (GB) equations (#1 and #4, respectively) are relatively the best fitting equations to the set of "*x–t*" data obtained at 800 °C. These two rate law equations were maintained to be the best fitting equations to the "*x–t*" data obtained at the other three test temperatures (700 °C, 750 °C and 850 °C). It is worth emphasizing, however, that the Ginstling–Brounstein (GB) equation is the corrected form of the rather empirical Jander (J) equation.

Rate constant values determined by Jander and Ginstling–Brounshtein rate law equations (Table 1) were used to construct Arrhenius plots (ln *k* vs. 1/*T*) for the reaction, and values of the activation energy (ΔE) and the frequency factor (*A*) therefrom derived are given in Table 2. It is

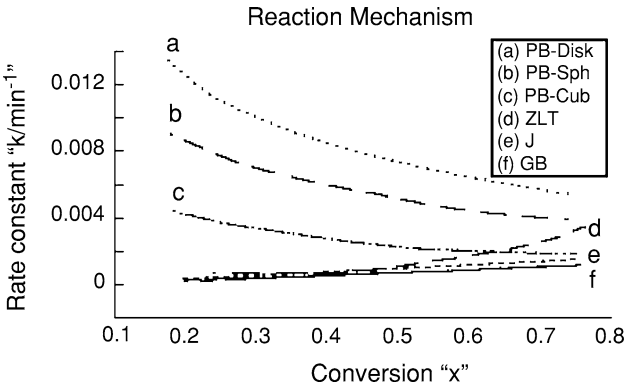

Fig. 2 Plots of reaction rate constant (*k*) values, determined via processing of *x–t* data obtained at 800 °C using the isothermal rate law equations indicated (and listed in Table 1), versus fraction of reaction completed in equimolar powder mixture of $BaCO_3$ and WO_3

Table 2 Isothermal and non-isothermal kinetic parameters

Isothermal				Non-isothermal[a]		
$\Delta E/\pm$ 2 kJ mol^{-1}		A/min^{-1}		$\Delta E/\pm$ 2 kJ mol^{-1}	*A*/min	Order[b]
J[c]	GB[d]	J[c]	GB[d]			
125	118	14.9×10^2	4.9×10^2	245	2×10^{10}	0.6

[a] Applying Ozawa's method [14–16]

[b] Order of reaction

[c] J = Jander equation (#1; Table 1)

[d] BG = Ginstling–Brounstein equation (#4; Table 1)

obvious from the table, that values of the isothermal kinetic parameters (ΔE and A) are not identical, but are rather reasonably close, particularly those of the activation energy (125 ± 2 (J-equation) and 118 ± 2 (GB-equation) kJ mol^{-1}). To the best of our knowledge, no such kinetic analysis results have been reported in the accessible literature for solid-state reactions in powder mixtures of $BaCO_3$ and WO_3.

Non-isothermal kinetic analysis of the reaction was carried out by processing of "x–T" data determined by TG curves obtained at four different heating rates, namely $\Phi = 10$, 20, 35 and 50 °C. According to Ozawa's method [14–16], slope of plots of "logΦ versus $1/T$" were used to determine the activation energy (ΔE) value corresponding to each of four different "x" values, namely $x = 20$, 40, 60 and 80%. The average value ($\Delta E = 245 \pm 2$ kJ/mol) thus obtained is shown (Table 2) to be almost twice as much as the isothermal activation energy value (118–125 kJ/mol). This significant disagreement can be largely alleviated when the energy data obtained at $x > 40\%$ are disqualified for being corresponding to the second and much faster reaction step, which was not involved in the isothermal energy calculations. Hence, the average of the two activation energy values corresponding to $x = 20$ and 40% was found to be (132 kJ/mole) much closer to the isothermal kinetic activation energy values (Table 2).

Incorporating the average non-isothermal ΔE value (=245 kJ/mol), the x–T data were processed by means of the following Eq. 12 to construct corresponding relationships of "dC/dθ versus θ", where $C = x$ and $\theta =$ reduced time [19].

$$d^2C/dt^2 = \left[d^2f(\theta)/d\theta^2\right]A^2[\exp(-2\Delta E/RT)] + (\Phi A\Delta E)/RT^2[df(\theta)/d\theta]\exp(\Delta E/RT) \quad (1)$$

The relationships thus obtained were automatically matched with theoretical relationships of preset reaction order and frequency factor "A" [14–16]. The closest matching encountered communicated the reaction order given in Table 2. Implementing Ozawa's algorithm [14–16], hypothetical "x–t" plots were calculated and constructed, and the reaction rate constant "k" at some selected temperatures in the reaction course was determined. When the k–T data thus obtained were used to construct an Arrhenius plot, the slope of which led to a closer activation energy value (164 kJ/mol) to the isothermal ones (118–125 kJ/mol) than the non-isothermal activation energy (245 kJ/mole).

It is obvious from the above kinetic handling, that the isothermal kinetic parameters, whether obtained directly by means of the best fitting isothermal rate law equations (Table 1) or indirectly within the framework of Ozawa's method, are more credible than the non-isothermal parameters. This is particularly true when the reaction course is a straightforward one, or involves chemically and/or kinetically resolved reaction steps. Accordingly, the solid-state reaction between $BaCO_3$ and WO_3 particles may be kinetically controlled by diffusion of reactants across the product(s) layer, which is shown to be best described by the isothermal rate law equation #4 (GB, Table 1) or equation #1 (J, Table 1) Fig. 2.

Reaction product analysis and mechanism

Calcination products of the separate and mixed reactants $BaCO_3$ and WO_3, obtained following heating in air at some selected temperatures in the reaction course (600–1,000 °C) for 3 h, were subjected to XRD, IR, LRa, SEM and EDS analyses. The results obtained were unanimous in indicating the following: (i) at <700 °C, the reaction powder mixture did not give rise to detectable indications of product formation, the sole detectable phases being the reactants $BaCO_3$ and WO_3, (ii) at 700 °C, weak XRD, IR and LRa diagnostic features of $BaWO_4$ commenced to emerge, (iii) at 750 °C, the reaction mixture was shown to contain $BaWO_4$ as the major component and WO_3 as the minor one, with no sign of the presence of $BaCO_3$, and (iv) at ≥850 °C, nothing was detectable in the reaction mixture, but $BaWO_4$. XRD, IR and LRa characteristics of the sole detectable product $BaWO_4$ in $BaWO_x$(850) are exhibited in Fig. 3. The XRD peaks are strong and narrow, which indicate formation of large crystallites of $BaWO_4$. The interplanner (d) spacings thus determined and the relative peak intensities displayed (Fig. 3) are very close to those filed in JCPDS 8-457 for tetragonally-structured $BaWO_4$. The four strongest XRD peaks correspond to the following d and (hkl) indices: 3.387 Å (112), 2.260 Å (204), 2.112 Å (220), and 1.715 (312). The fact that the peak at $d = 2.260$ Å is shown to be slightly more intense than the latter two peaks may be considered, according to Xie et al. [4], to be indicative of a slight monoclinic distortion of the product tetragonal lattice. In line with these XRD results, the LRa spectrum of $BaWO_x$(850) displays nothing but the characteristic peaks of $BaWO_4$ [20, 21] (Fig. 3). The same applies to corresponding IR spectrum (Fig. 3), though it shows in addition to the strongly overlapping absorptions of W–O lattice vibrations (at 919–798 cm^{-1}) of tungstate groups of $BaWO_4$ [22–24] a very weak and broad band at 1,429 cm^{-1}, which could be due to impurity carbonate species.

The SEM micrograph obtained for $BaWO_x$ (850), Fig. 4(a), reveals agglomerates, in a rather perfect egg-shell structure of large diameters (50–60 μm and 70–80 μm), of polyhedral crystallites of uniform edge length in the range 2–3 μm (Fig. 4b), when the x-labeled particle shown in

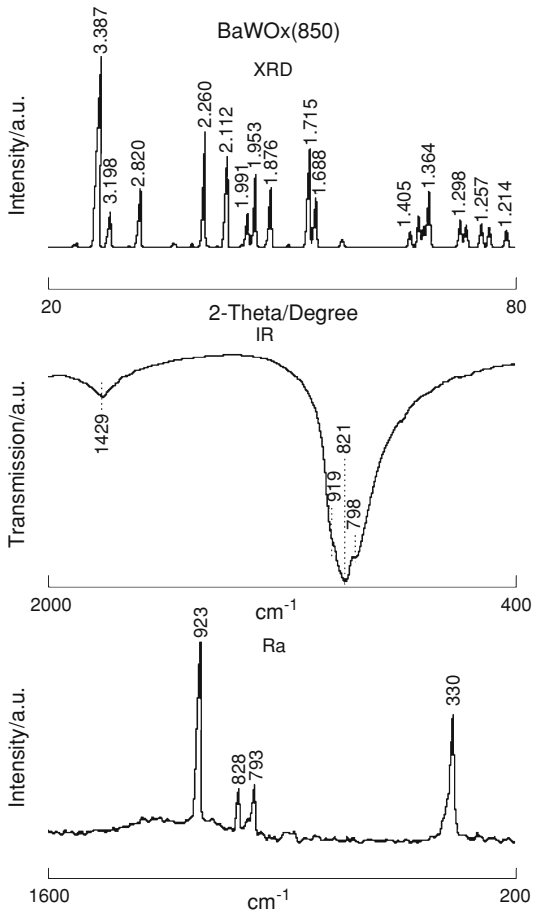

Fig. 3 XRD diffractogram, and IR and LRa spectra exhibited by the equimolar powder mixture of $BaCO_3$ and WO_3 following its calcination at 850 °C for 3 h. The diffraction peaks are indicated by the corresponding *d*-spacing values (in Å)

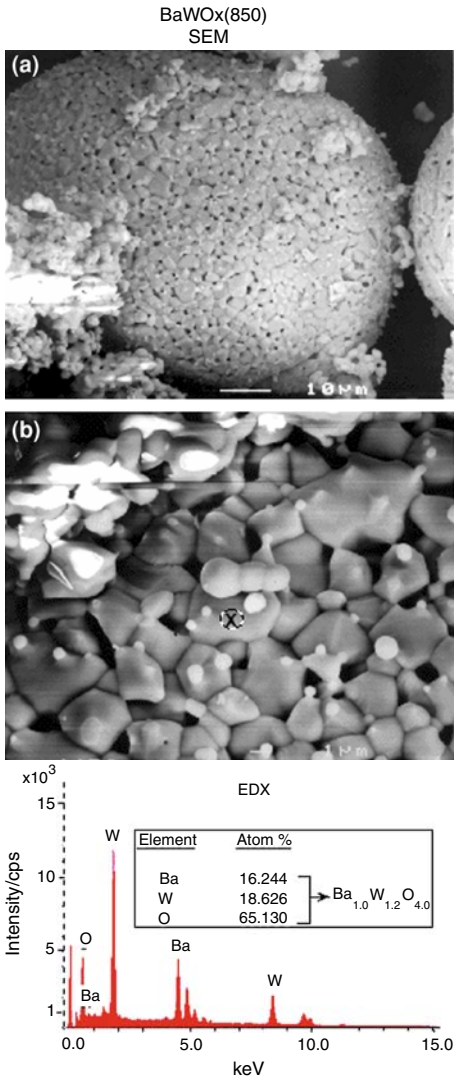

Fig. 4 SEM micrographs obtained (at two different magnifications) for the equimolar powder mixture of $BaCO_3$ and WO_3 following its calcination at 850 °C for 3 h. The EDX micro-probing results were obtained for the x-labeled location of the micrograph (**b**)

Fig. 4b was EDS-analyzed, the results reported in Fig. 4 were obtained. These results communicate detection of Ba, W and O atoms in proportions making-up the empirical formula $Ba_{1.0}W_{1.2}O_{4.0}$. This formula is, indeed, indicative of formation of $BaWO_4$ crystals, provided that the extra-formula amount of W is due to inaccurate quantification of the element caused by overlapping contribution from Ba L-series [25]. This morphology, evolving in the solid state, is entirely different from the morphologies observed for $BaWO_4$ particles synthesized in solutions containing different surfactants [4]. Xie et al. [4] have reported that different surfactants can form micelles with different morphologies, and, hence, olive-like, flake-like and whisker-like $BaWO_4$ crystals were prepared. These authors [4] could, however, show that increasing concentration of the parent materials ($BaCl_2$ and Na_2WO_4) in solutions containing one-and-the same surfactant results in $BaWO_4$ crystals of polyhedral-like morphology, i.e. similar to the present case (Fig. 4b).

The above results may imply that the product layer, $BaWO_4$, must have been established on the carbonate particles. Accordingly, one may suggest the migration of WO_3 species towards the carbonate particles to trigger the formation reaction of the tungstate:

$$BaCO_3 + WO_3 \rightarrow BaWO_4 + CO_2 \uparrow$$

Using a set of similar powder mixtures of WO_3 and MCO_3, where M stands for Mg, Ca, Sr or Ba, Guo and Kleppa [26] have determined enthalpy of formation of each corresponding tunhstate (MWO_4) by high-temperature direct synthesis calorimetry. They have determined enthalpy of formation of -256 ± 3.9 kJ/mol (at 298 K) for $BaWO_3$. They, moreover, concluded that the magnitude

of the enthalpy of formation of MWO_4 increases almost linearly with the increase of the ionic radius of the divalent cation, and suggested migration of WO_3 species towards $BaCO_3$ particles to trigger the reaction [26]. In the exothermic direction of the reaction, the increase of the heat of formation would be corresponded by a decrease of the activation energy of the reaction [27]. Hence, the high enthalpy of formation observed for $BaWO_4$ [26] would favour the low isothermal activation energy (118–125 kJ/mol) over the high non-isothermal activation energy (245 kJ/mole) determined in the present work for the formation reaction of $BaWO_4$.

The mass loss (10.25%) theoretically anticipated upon completion of the formation reaction of $BaWO_4$ is very close to the TG-determined mass loss (10.1%) for the reaction (Fig. 1). In view of the facts that (i) $BaWO_4$ is the raction sole detectable product, and (ii) its rate is diffusion controlled, occurrence of the mass loss accompanying the reaction via two kinetically resolved steps (Fig. 1) may account for a high-temperature alleviation of the diffusion control at >943 °C (Fig. 1). In other words, if the slow rate of the reaction at <943 °C is attributed to the usually slow diffusion of reactants across the product layer, the marked enhancement observed at >943 °C (Fig. 1) might be ascribed to a change in the nature of the rate determining process from a physical to a chemical one. Thus a proportional, considerable enhancement of the diffusion rate must be expected.

The reaction interface may, accordingly, be envisaged to assume the following phase composition: $BaCO_3|BaWO_4|WO_3$, with, most likely, a unidirectional diffusion of WO_3 species, through the product layer, towards the carbonate. The present results cannot help concluding the nature of the diffusing tungesta species, i.e. whether cationic diffusion and "oxygen-vapour" transport [27] or "$WO_x(OH)_y$-vapour" transport. Admittedly, however, formation of volatile $WO_x(OH)_y$ species is much less likely than the analogous $MoO_x(OH)_y$, which is known to form when MoO_3 is heated in a wet atmosphere [28]. On the other hand, cationic diffusion is supposed to take place via interstitial voids [13, 27] of the lattice of a product layer, i.e. it is a structure-sensitive process. Oxygen-vapour transport, on the other hand, is controlled by the energy required to release oxygen into the vapour phase [13], and subsequently by the conjugate electronic mobility through the product layer maintaining local electrical neutrality. It is plausible to suggest, that a change of nature of the diffusing species across a given product layer, or a change of the product layer accessibility to a given diffusing species, may explain the observed change in the reaction rate as a function of temperature (Fig. 1). Unfortunately, the present results cannot help favouring either of these alternatives.

Conclusions

The above presented and discussed results may help drawing the following conclusions:

1. The chemical reactivity is triggered in equimolar powder mixture of $BaCO_3$ and WO_3 near 465 °C in air, producing $BaWO_4$ in the solid state and releasing CO_2 into the gas phase.
2. The formation of the tungstate at a temperature range (<943 °C) at which the separate reactants are thermally stable, together with the absence of formation of separate BaOx species in the reaction course, provide sufficient evidence for the concurrence of CO_2 release to the formation reaction of $BaWO_4$.
3. Ginstling–Brounshtein ($k_{BG}\ t = 1 - 2x/3 - (1-x)^{2/3}$) and Jander ($k_J\ t = [1 - (1-x)^{1/3}]^2$) rate law equations are best describing the isothermal kinetic data, thus indicating that the reaction rate (i.e., product formation) is controlled by diffusion of reactants across the product layer.
4. The diffusing reactant species may be those of WO_3, which may migrate either in the form of cationic diffusion and oxygen-vapour transport, or $WO_x(OH)_y$-vapour transport. Though formation of such latter $WO_x(OH)_y$ volatile species is less likely, it cannot be excluded with certainty.
5. Despite some obvious shortcomings, non-isothermal kinetic measurements can enable steps in the reaction course to be distinguished.

Acknowledgements The financial support facilitated by the College of Post-graduate Studies, and the excellent technical support found at SAF and EMU of the Faculty of Science of Kuwait University are highly appreciated

References

1. Blasse G, Schipper WJ. Phys Status Solidi A. 1974;25:163.
2. Blasse G, Dirksen GJ. J Solid State Chem. 1981;36:1267.
3. Mitsubishi Mining and Cement Co., Japanese Patent, Jpn. Kokai Tokyo Koho (1985), JP 83-195318 19831020.
4. Xie B, Wu Y, Jiang Y, Li F, Wu J, Yuan S, et al. J Cryst Growth. 2002;235:283.
5. Cho WS, Yoshimura M. Jpn J Appl Physics A. 1997;36:1216.
6. Kwan S, Kim F, Akana J, Yang P. Chem Commun. 2001;5:447.
7. Grigorieva TF, Vorsina IA, Barinova AP, Korchagin MA, Lyakhov NZ. J Mater Synth Processing. 2000;8:339.
8. Zyryanov VV. Inorg Mater. 2000;36:54.
9. Mamykin PS, Batrakov NA. Tr Ural Politekh Inst. 1966;150:101.
10. Kislyakov IP, Mel'nikov AI, Sokolovskaya RV, Tokunov OI. Izv Akad Nauk SSSR, Neorg Mater. 1966;2:1467.
11. Shurdumov GK, Shurdumov ZV, Cherkesov ZA, Karmokov AM. Russ J Inorg Chem. 2006;51:531.
12. Al-Hajji LA, Hasan MA, Zaki MI. J Mater Res. 2003;18:2339.
13. Hulbert SF, Klawitter JJ. J Am Ceram Soc. 1967;50:484.
14. Ozawa T. Bull Chem Soc Jpn. 1965;38:1881

15. Ozawa T. J Thermal Anal 1970;2:301
16. Ozawa T. Thermochim Acta 1992;203:159.
17. Sestak J, Berggren G. Thermochim Acta. 1971;3:1.
18. Heide K, Höland W, Gölker H, Seyfarth K, Müller B, Sauer R. Thermochim Acta. 1975;13:365.
19 Zhang JJ, Ge LG, Zha XL, Dai YJ, Chen HL, Mo LP. J Thermal Anal Cal. 1999;58:269.
20. Stencel JM. Raman spectroscopy for catalysts. New York: Van Norstrand Reinhold; 1990.
21 Degen IA. Tables of characteristic group frequencies for the interpretation of infrared and raman spectra. Harrow Weald: Acolyte Publ; 1997.
22. Nakamoto K. Infrared and Raman spectra of inorganic and coordination compounds. 5th ed. Chichester: Wiley; 1977. p. 180–4.
23. Nyquist RA, Kagel RO. Infrared spectra of inorganic compounds. New York: Academic Press; 1971.
24. Miller FA, Carlson GL, Bently FF, Jones WH. Spectrochim Acta. 1960;16:135.
25. Röntec GmbH, Application Report and Private Communication, Berlin. 2000.
26. Guo Q, Kleppa OJ. Thermochim Acta. 1996;288:53.
27. Schmalzried. Chemical kinetics of solids. Weinheim: VCH-Verlag; 1995.
28. Glemser O, van Hässeler R. Z Anorg Allg Chem. 1962;316:168.